



Insights into active deformation in the Gulf of Cadiz from new 3-D seismic and high-resolution bathymetry data

Gareth J. Crutchley

Leibniz Institute of Marine Sciences at the University of Kiel (IFM-GEOMAR), Wischhofstrasse 1-3, D-24148 Kiel, Germany (gcrutchley@ifm-geomar.de)

Christian Berndt

Leibniz Institute of Marine Sciences at the University of Kiel (IFM-GEOMAR), Wischhofstrasse 1-3, D-24148 Kiel, Germany

National Oceanography Centre, Southampton, European Way, Southampton SO14 3ZH, UK

Dirk Klaeschen

Leibniz Institute of Marine Sciences at the University of Kiel (IFM-GEOMAR), Wischhofstrasse 1-3, D-24148 Kiel, Germany

Doug G. Masson

National Oceanography Centre, Southampton, European Way, Southampton SO14 3ZH, UK

[1] The nature of active deformation in the Gulf of Cadiz is important for developing a better understanding of the interplate tectonics and for revealing the source of the 1755 Great Lisbon earthquake. New, high-resolution 3-D seismic data reveal a classic pull-apart basin that has formed on an east striking fault in the Southern Lobe of the Gulf of Cadiz accretionary wedge. Geometrical relationships between an array of faults and associated basins show evidence for both dextral and sinistral shear sense in the Southern Lobe. Strike-slip faulting within the lobe may provide a link between frontal accretion at the deformation front and extension and gravitational sliding processes occurring further upslope. Inception of the strike-slip faults appears to accommodate deformation driven by spatially variant accretion or gravitational spreading rates, or both. This implies that active deformation on strike-slip faults in the Southern Lobe is unrelated to the proposed modern inception of a transform plate boundary through the Gulf of Cadiz and underscores the importance of detailed bathymetric analysis in understanding tectonic processes.

Components: 9900 words, 11 figures.

Keywords: 3-D seismic imaging; Gravitational sliding; Gulf of Cadiz; Lisbon Earthquake; Pull-apart basin.

Index Terms: 3025 Marine Geology and Geophysics: Marine seismics (0935, 7294); 3045 Marine Geology and Geophysics: Seafloor morphology, geology, and geophysics; 8122 Tectonophysics: Dynamics: gravity and tectonics.

Received 23 February 2011; **Revised** 6 June 2011; **Accepted** 6 June 2011; **Published** 22 July 2011.

Crutchley, G. J., C. Berndt, D. Klaeschen, and D. G. Masson (2011), Insights into active deformation in the Gulf of Cadiz from new 3-D seismic and high-resolution bathymetry data, *Geochem. Geophys. Geosyst.*, 12, Q07016, doi:10.1029/2011GC003576.



1. Introduction

[2] The Gulf of Cadiz is a geologically complex region situated offshore Southwest Iberia and Northwest Morocco, at the boundary between the Eurasian and African plates (Figure 1a). The location of the plate boundary between Africa and Iberia and further west into the Gulf of Cadiz is difficult to constrain due to diffuse seismicity and broad regions of complex deformation [Calvert *et al.*, 2000; Gutscher *et al.*, 2009b; Sartori *et al.*, 1994; Tortella *et al.*, 1997]. The tectonic nature of the recent plate boundary is the topic of much debate. Platt and Vissers [1989] proposed a geodynamic model of delamination of continental lithosphere beneath the Alboran Sea region to explain the radial pattern of thrusting around the Gibraltar Arc and the extensional basin at its center – structural patterns that are difficult to explain by simple interplate convergence that has been ongoing since the Mid-Oligocene [Dewey *et al.*, 1989; Medialdea *et al.*, 2009; Rosenbaum *et al.*, 2002]. Alternatively, Lonergan and White [1997] suggested that coeval extension and shortening resulted from a subduction zone which rolled back until it collided with North Africa. Gutscher *et al.* [2002] proposed that subduction is actively ongoing and that the hummocky region enclosed by a horseshoe-shaped deformation front that dominates much of the central gulf (highlighted in Figure 1a) is the seafloor expression of an active accretionary wedge. Zitellini *et al.* [2009], in an evaluation of a new compilation of bathymetric data, have interpreted a series of ESE striking dextral strike-slip faults (the “SWIM faults”) that they suggest represent a modern transform plate boundary through the Gulf of Cadiz. Strong earthquakes that have occurred in the Gulf of Cadiz, including the M8.7 Great Lisbon earthquake that caused near total destruction of Lisbon in 1755, have driven much of the research into characterizing the plate boundary through this region in order to better constrain the nature of seismic hazard in Iberia and northern Africa [e.g., Gràcia *et al.*, 2003; Gutscher, 2004; Terrinha *et al.*, 2003; Zitellini, 2001].

[3] In the current study, we use high-resolution 3-D seismic data and swath bathymetry data to characterize a classic pull-apart basin associated with a prominent strike-slip fault that branches off one of the SWIM faults interpreted by Zitellini *et al.* [2009]. The fault and basin are situated within the

Southern Lobe of the upper part of the accretionary wedge, as interpreted by Gutscher *et al.* [2009a] (Figure 1a). We use a new compilation of bathymetric data sets [Gutscher *et al.*, 2009b; Zitellini *et al.*, 2009] together with the tectonic interpretation of the seismic data to shed new light on the nature of active deformation within the upper part of the accretionary wedge.

[4] In addition to the regional tectonic implications, detailed interpretation of the seismic data gives new insight into the 3-D structure of actively deforming pull-apart basins. The imaging and interpretations provide an excellent natural example of pull-apart basin architecture that yields the opportunity for comparison with other pull-apart basins and existing analog modeling results.

2. Data

[5] High-resolution 3-D seismic data were acquired in the Gulf of Cadiz during March and April of 2006 as part of an international research program investigating Europe’s deep marine ecosystems and their environment – the HERMES project (Hot spot Ecosystem Research on the Margins of European Seas). The data of this survey (Cruise CD178) were acquired using the RRS Charles Darwin of the National Environment Research Council (NERC) and the P-Cable 3-D acquisition system of the National Oceanographic Centre, Southampton (NOCS). The P-Cable consists of a cross wire extended perpendicular to the ship’s steaming direction that is held in place by paravanes attached to both ends of the wire. In a normal setup of this system, 12 single-channel Teledyne Instruments analog streamers are connected to the cross wire and towed parallel to the ship’s steaming direction. In Cruise CD178, only 11 streamers were used due to a defective streamer. The streamers were towed at a depth of approximately 1 m, with inline spacing between adjacent streamers of approximately 12 m. The source consisted of four 40 in³ Bolt 600B air guns spaced 0.75 m apart and towed at a depth of 1.5 m about 20 m behind the stern of the vessel. The average shot spacing was ~10 m, with a sample rate of 1 ms and a dominant frequency of ~80 Hz. The seismic cube presented in this study is a 10 km² survey designed to cover the basin shown in the bathymetry data of Figure 1b. In addition to seismic data, we present high-resolution bathymetry data that were collected using the SIMRAD EM120 multi-

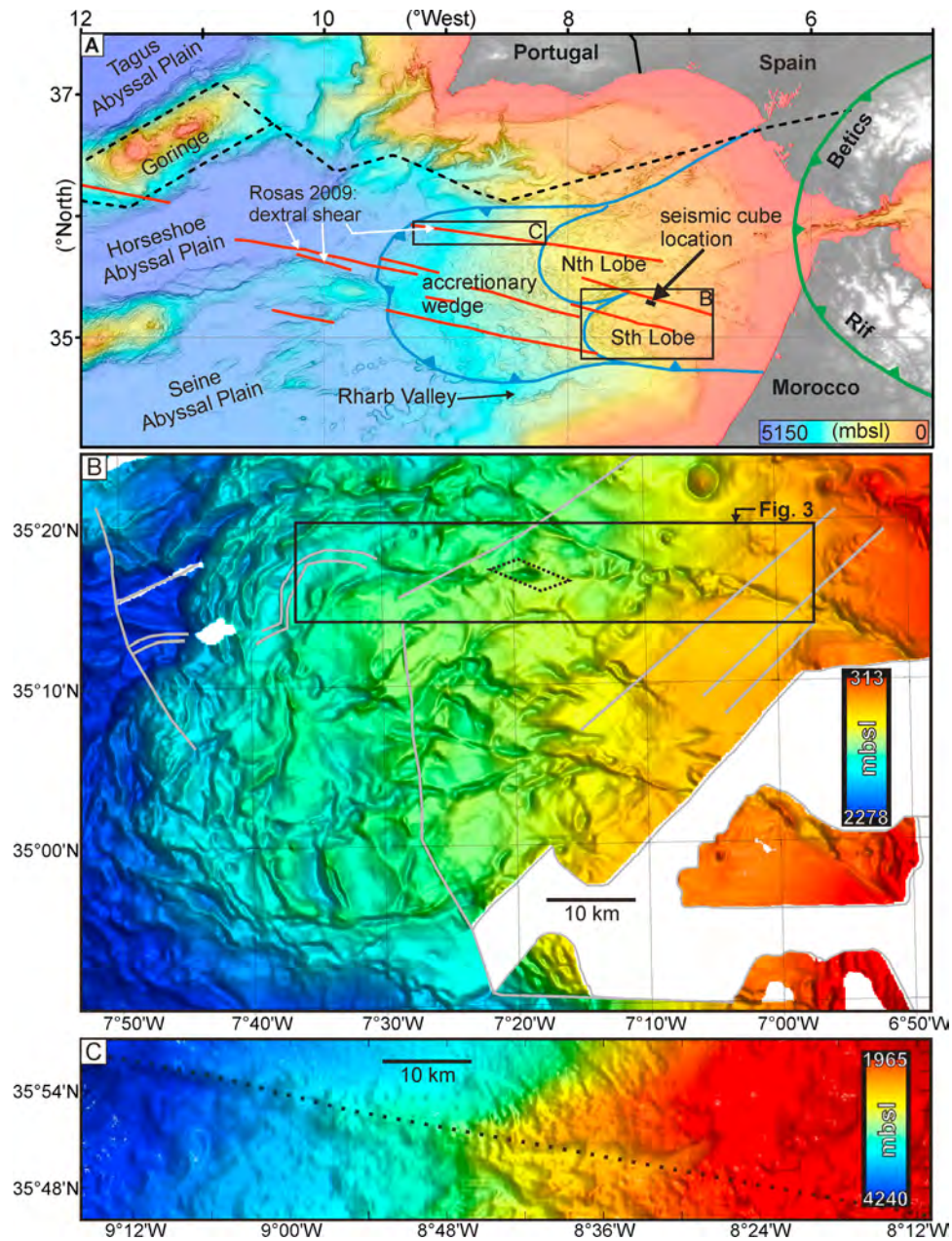


Figure 1. (a) Regional map of the Gulf of Cadiz. Gaps in the high-resolution data set [Zitellini *et al.*, 2009] have been filled with lower-resolution data from the General Bathymetric Chart of the Oceans (GEBCO). The approximate position of the plate boundary (based on seismicity) between the African Plate to the south and the Eurasian Plate to the north (dashed black line) and the outline of the accretionary wedge and its interior Northern and Southern Lobes (blue lines) are from Gutscher *et al.* [2009a]. The red lines are the so-called “SWIM” dextral strike-slip faults [after Zitellini *et al.*, 2009]. Dextral shear modeled by Rosas *et al.* [2009] on SWIM segments immediately NW of the accretionary wedge (white arrows). (b) Illuminated high-resolution bathymetry data from the black box surrounding the Southern Lobe in Figure 1a. The GMT “*grdgradient*” function was used to apply Lambert diffuse lighting and specular highlights to the bathymetric surface with a lighting azimuth of 360° and an elevation angle of 30°. Data gaps are “blacked out” by gray lines. The black box shows the extent of view given in Figure 3. The dotted black quadrilateral within the black box shows the areal coverage of the seismic cube. (c) Illuminated high-resolution bathymetry data from the black box west of the Northern Lobe in Figure 1a. This image is plotted at the same scale as Figure 1b, with the same illumination methods. The black dotted line delineates one of the interpreted dextral strike-slip SWIM faults [after Rosas *et al.*, 2009; Zitellini *et al.*, 2009].



beam bathymetry system (nominal frequency of 12 kHz) during the same cruise.

3. Bathymetry Processing Methods

[6] The bathymetric data acquired during Cruise CD178 were merged with a high-resolution regional data set that has been presented in recent studies of the Africa-Eurasia plate boundary in the Gulf of Cadiz [Gutscher *et al.*, 2009b; Zitellini *et al.*, 2009]. The merged data set was used to relate our seismic cube to regional seafloor morphology. In order to interpret seafloor features, different spatial analyses were carried out in Matlab and ArcGIS to produce attribute maps that provide insight into various morphological characteristics.

[7] Slope angle maps were calculated to highlight steep sections of the seafloor that are useful for the localization of geological features such as fault traces, mud volcanoes and channel systems. Profile and plan curvature maps were calculated to highlight curvature variation along the direction of steepest gradient and the direction of the contours, respectively. The former, therefore, highlights along-slope ridges and crests, whereas the latter highlights downslope ridges and crests [e.g., Micallef *et al.*, 2007; Wilson *et al.*, 2007]. In addition to the attribute analysis techniques described above, several illumination methods (including hill shades, Lambert diffuse lighting, and specular highlights [Wessel and Smith, 1998]) were used in the viewing of bathymetric surfaces.

4. Seismic Processing Methods

[8] The geometry of the P-Cable acquisition is controlled by GPS antennae that track the positions of the doors and the guns. The positions of each of the 11 channels on the streamers were calculated geometrically from the known connection points of the streamers on the cross wire and by approximating the shape that the cross wire forms as it is towed through the water. The predicted geometry for each shot was then fine-tuned to account for first arrival times on each channel that were inverted to source-receiver offset using water velocity. We tested both triangular and catenary curve geometrical configurations of the cross wire and found, based on first arrival times, that catenary curves offered a slightly better approximation of the true geometry. However, it is noted that the differences were sufficiently small that after CDP binning into 10 m bins there was no difference in

the fold map. The geometry was then “fine-tuned” by moving the geometrically predicted positions by small amounts either toward the ship or away from the ship, depending on the calculated source-receiver offset from the first arrival times. That is, if the first arrival time yielded a distance greater than the offset from the source to the predicted receiver on the catenary curve, the receiver would be moved away from the ship by the amount of the discrepancy. The resulting geometry was subsequently used for CDP sorting into bins with dimensions of 10 m by 10 m in the cross-line and in-line directions, respectively.

[9] Swell noise in each of the 11 channels was reduced by picking the seafloor reflection and low-pass filtering of swell-related trace to trace fluctuations. This process achieved a marked improvement in the coherency of the seafloor and subseafloor reflections. In addition to this time domain filtering, data were filtered in the frequency domain to remove low frequency noise and were then corrected for the effect of geometrical spreading. Data were subsequently corrected for normal move out (assuming a constant velocity of 1500 m s^{-1}) before being stacked to form the cube.

[10] The complex and deformed geology of the pull-apart structure resulted in numerous diffractions that needed to be collapsed by migration to reveal as much as possible of the structural complexity. Close inspection of the poststack unmigrated cube revealed spatial aliasing of steeply dipping diffractions. To circumvent this problem, we incorporated trace interpolation routines to increase the spatial sampling of data from a 10 m by 10 m trace spacing (in-line spacing by cross-line spacing) to a 5 m by 5 m trace spacing. We tested both a 3-D trace interpolation and a 2-D interpolation that works by summing existing adjacent traces that have been time-shifted by various amounts such that they line up at the angles of maximum coherency. A 3-D application of the 2-D interpolation (i.e., first executed in the cross-line direction, then in the inline direction) yielded better results. These data were then stacked and migrated with a 3-D Kirchhoff algorithm incorporating a constant 1500 m s^{-1} velocity model.

[11] In order to extract as much structural information from the data as possible, a “similarity” data set was calculated from the final seismic cube with the OpenDtect seismic interpretation program. Similarity is a measure of the trace-to-trace coherency calculated throughout the 3-D volume. This coherency expresses how much two or more trace



segments look alike. A similarity of 1 means that the trace segments are identical and a similarity of 0 means that they are completely dissimilar.

5. Bathymetric Imaging and Interpretations

[12] The accretionary wedge complex has a very rough seafloor expression, especially when compared with the directly surrounding Seine Abyssal Plain and Rharb valley [Gutscher *et al.*, 2009a] (Figure 1). The distribution of steep slope angles within the complex indicates focused deformation around its southern margin (i.e., immediately north of the Rharb Valley) and around two internal portions referred to as the Northern and Southern Lobes [Gutscher *et al.*, 2009a] (Figure 1a). The reader is referred to Gutscher *et al.* [2009a] for the regional distribution of slope angles.

[13] The addition of the CD178 bathymetry data to the regional compilation allows us to constrain the surface manifestation of deformation in the Southern Lobe. The first observation that was immediately evident was that deformation lineaments in the Southern Lobe have a much more sharply defined, “fresh” appearance than deformation lineaments further west in the Gulf of Cadiz. This fresh appearance, interpreted as indicating a youthful origin, is especially apparent when comparisons are made (for example) to the dextral strike-slip faults studied by Rosas *et al.* [2009], located several hundred kilometers to the WNW. Figures 1b and 1c, plotted at the same scale from the same bathymetry set, highlight this pronounced difference in appearance: Figure 1b, from the Southern Lobe, and Figure 1c from one of the dextral strike-slip faults interpreted by Rosas *et al.* [2009]. The fabrics in the Southern Lobe appear, therefore, to be significantly younger than interpreted strike-slip faults farther west in the Gulf of Cadiz.

[14] Shaded relief maps (e.g., Figure 1b) and slope maps (Figure 2a) were used to map prominent seafloor lineations and make a thorough interpretation of bathymetric morphology within the Southern Lobe (Figure 2b). Clearly, the roughest part of the Southern Lobe is its toe region, where steep slopes define the surface expression of focused, active deformation (deformation front highlighted green in Figure 2b) [Gutscher *et al.*, 2009a]. The arcuate shape of the deformation front, and also of other lineations to the east, resembles the surface expressions of push-up rid-

ges that may be caused by either thrusts or blind thrusts. This is supported by a bathymetric profile extracted from west of the deformation front to the central reaches of the eastern part of the lobe (Figure 2h), showing the prominent topographic high to the east of the deformation front and the rugged seafloor terrain that continues approximately 15 km eastward from the deformation front. The bathymetric data therefore indicate that thrust-style deformation continues eastward from the deformation front over a distance of approximately 10–20 km (pink shaded region east of the deformation front in Figure 2b). Shortening in this western part of the lobe is consistent with the interpretations of Gutscher *et al.* [2009a]. Further shoreward, in the eastern part of the lobe (shaded gray in Figure 2b), the seafloor is much flatter and smoother, but it is dissected by a series of lineations. Two of these pronounced lineations are the ESE striking SWIM strike-slip fault segments (red lines in Figure 2b), which are hereafter referred to as the Northern and Southern SWIM faults [Zitellini *et al.*, 2009]. Additionally, there is a dominant orientation of E to ESE striking faults that branch off the SWIM faults. Several basins (yellow regions in Figure 2b with extracted slope profiles in Figures 2c–2g) are identified along both the ESE striking and the east striking faults, and appear to be related to step overs. Therefore, we suggest that they are pull-apart basins: that is, that they have formed in response to transtension on strike-slip faults. Basin d and its hosting strike-slip fault are the basis of detailed discussion in this paper; we hereafter refer to them as the Hermes Basin and the Hermes Fault, respectively.

[15] Enlarged curvature plots of the bathymetry around the Hermes Fault reveal more clearly the lineations of both this fault and the adjoining Northern SWIM fault (Figure 3). The strong negative component of the plan curvature map (Figure 3a) sharply defines the fault traces on the seafloor – these are observed as the dark blue lineations. The strong positive (red) and strong negative (blue) components of the profile curvature map (Figure 3b) show where the profile is changing rapidly. This map highlights well the extent of the Hermes Basin, which is revealed by the region of strong positive and strong negative curvature (Figures 3b and 3c). The strong negative regions marked by blue streaks, defining rapidly changing concave-down curvature, highlight the margins of the basin (Figure 3c). The strong positive regions, defining rapidly changing concave-up curvature, highlight the perimeter of the basin floor (Figure 3c).

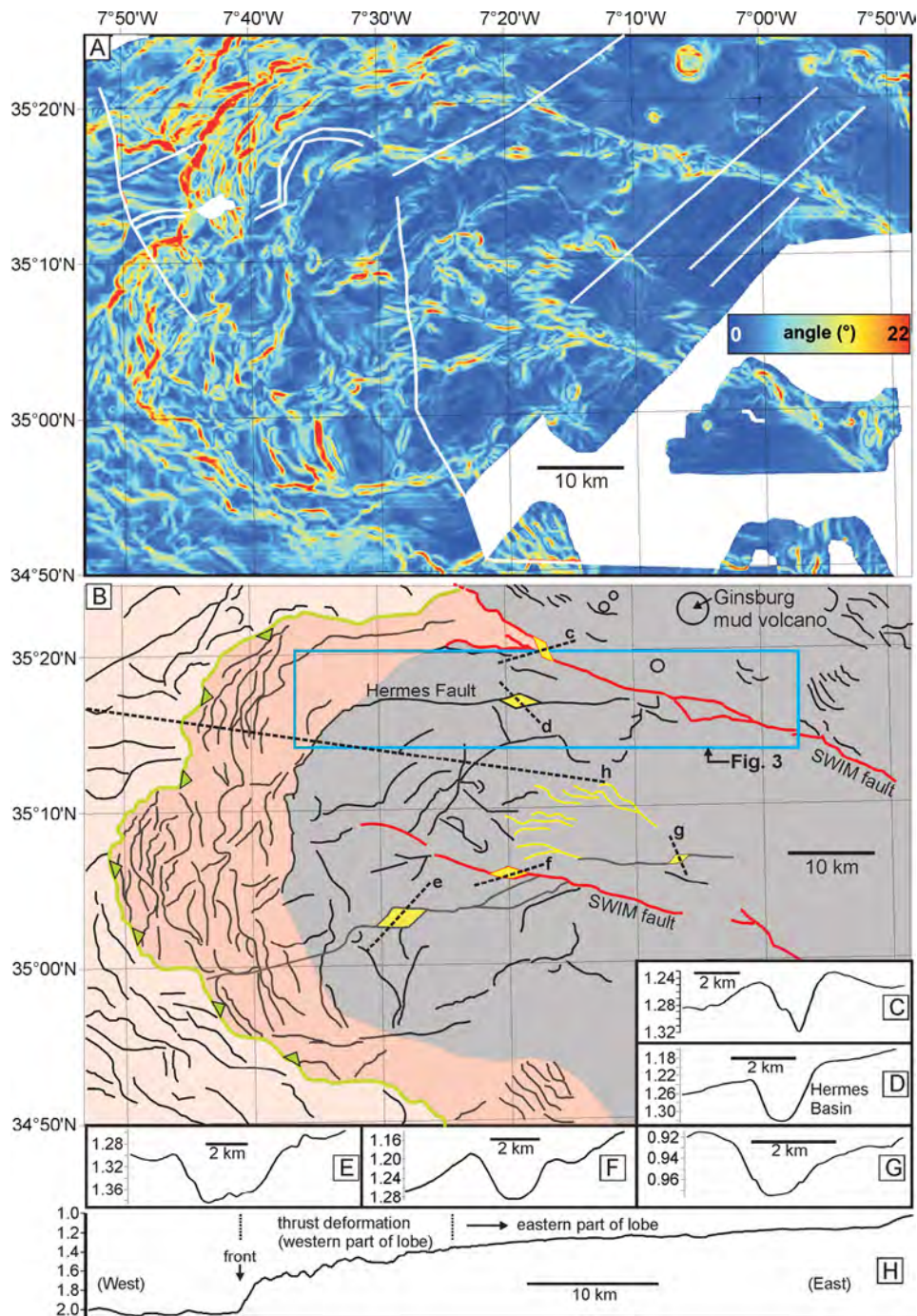


Figure 2. (a) Slope angle map (same map extent as Figure 1b). Steep slopes reveal various features, including the deformation front of the lobe, other accretionary fabrics, strike-slip faults, channel systems, and mud volcanoes. (b) Interpretation of prominent seafloor lineations revealed in Figure 2a and in Figure 1b. The prominent deformation front of the Southern Lobe (green line) separates the lower accretionary wedge (pale pink) from the lobe itself. The apparent extent of thrust-dominated deformation within the Southern Lobe is shaded darker pink. The eastern part of the lobe (gray) is dominated more by prominent sublinear faults, including the SWIM strike-slip faults (red lines). Also marked in the eastern part are (1) basins (yellow) that are interpreted to be caused by local pull-apart tectonics on strike-slip faults and (2) interpreted channels systems (sinuous yellow lines). All other lineations are marked black. The blue box shows the extent of the view given in Figure 3. (c–g) The extracted bathymetric profiles shown in Figure 2b by the positions of the dashed black lines transecting the basins. Note that profile d crosses the Hermes Basin – studied in greater detail with the 3-D seismic cube. (h) Bathymetric profile showing the deformation front, as well as the interpreted section of thrust deformation (western part of the lobe) and the smoother eastern part of the lobe.

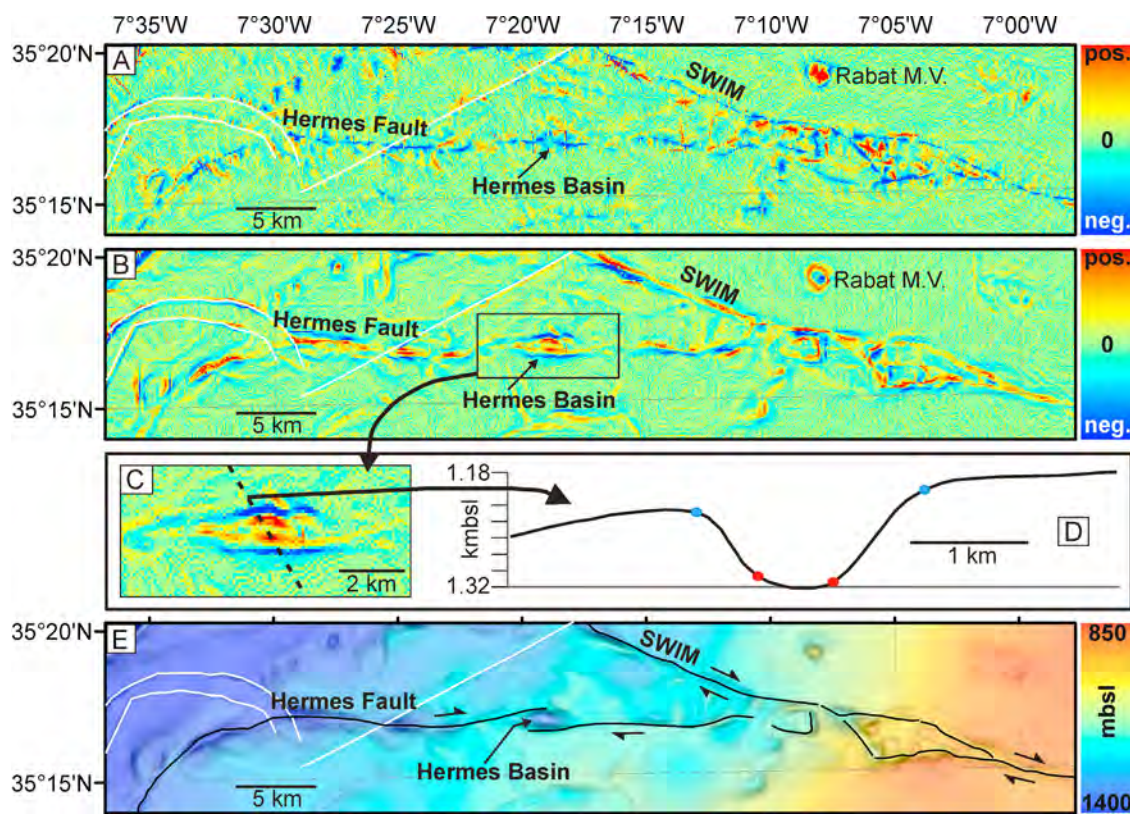


Figure 3. (a) Plan curvature map from the area highlighted by the blue box in Figure 2b. White regions blank out grid artifacts. Zero curvature (colored green) represents flat surfaces. Negative curvatures indicate that the surface is upwardly concave at the point of observation, whereas positive curvatures indicate a downwardly concave surface. Strong negative curvature (dark blue) highlights the east striking Hermes Fault and the ESE striking SWIM Fault. (b) Profile curvature map of the same area as in Figure 3a. Negative curvature indicates upwardly concave regions, and positive curvature indicates downwardly concave regions. (c) Enlarged region covering the Hermes Basin. The dashed line shows the location of the profile in Figure 3d. (d) Extracted profile through the basin. Blue and red dots show strongly negative and strongly positive curvature, respectively. (e) Shaded relief map of the same area as in Figures 3a and 3b with major lineations annotated. The Hermes Fault, like the SWIM Fault that it intersects in the region 7°7'W/35°17'N, is interpreted as dextral strike slip.

A bathymetric profile extracted through the basin (Figure 3d) shows the concave-down and concave-up curvature at the basin margins and basin floor, respectively. The interpretation of the pull-apart basin and its relationship to the Hermes Fault and the Northern SWIM fault is shown in Figure 3e. The Hermes Basin is interpreted to have formed as a result of a releasing bend on a dextral strike-slip fault. Seismic imaging presented later supports this interpretation.

[16] A clear contrast in the deformation style of the lobe was shown in Figure 2, from the accretionary style frontal part (shaded pink in Figure 2b) to the smoother eastern part that is multiply dissected by relatively linear fault traces (shaded gray in Figure 2b). In the west, the Hermes Fault bends southward forming an arcuate expression that

mimics the deformation front (Figures 2a and 2b). Thus, we interpret this bathymetric lineation to be the expression of a strike-slip fault in the eastern part of the lobe (Figure 3e) that bends southward and merges into a thrust feature associated with frontal deformation in the western part of the lobe (Figure 2b). This transition of the frontal accretion zone to strike-slip faulting further east is illustrated in the oblique 3-D view of Figure 4. The seafloor expressions of the ESE and east striking faults in the eastern reaches are seen to bend around and merge with the thrust ridges of the frontal deformation zone. Not only does the Hermes Fault exhibit this phenomenon, but also the SWIM fault immediately to the north, which bends around and merges with the deformation front. It is expected that a combination of reverse and shear motion is

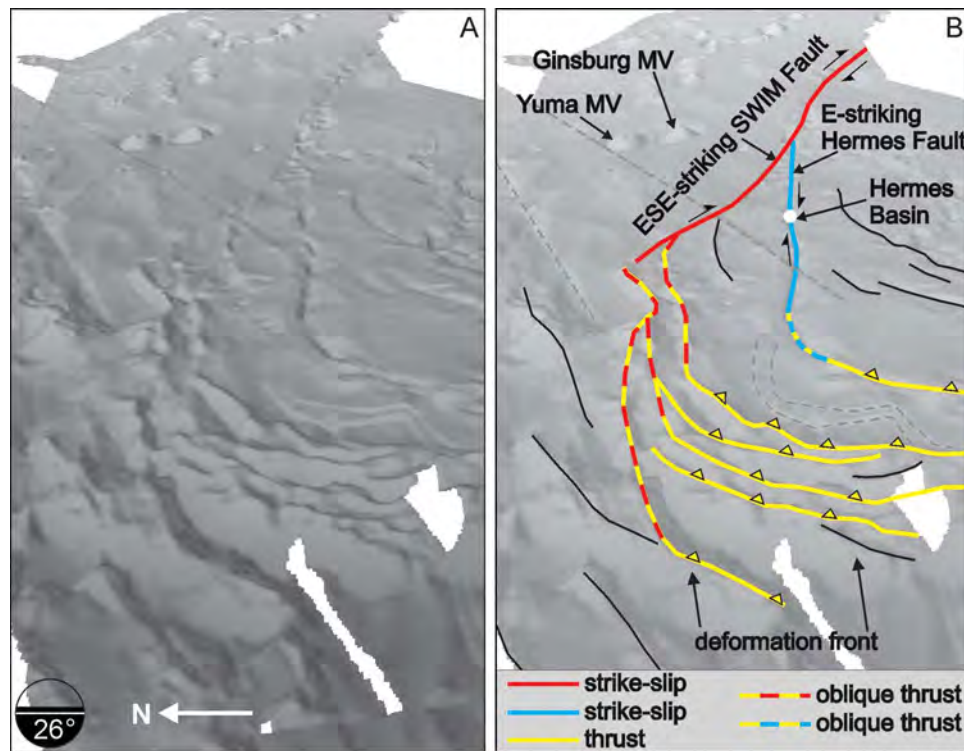


Figure 4. (a) Three-dimensional perspective view and (b) interpretation looking eastward from above the deformation front of the Southern Lobe of the accretionary wedge. The north arrow and the tilt meter to the lower left of Figure 4a describe the orientation of the view. Interpreted transition zones between the thrust deformation region (yellow lines) and the strike-slip faults (red and blue lines) are represented by dashed lines of alternating color. Dashed gray lines blank out grid artifacts.

accommodated along the segments of these structures that lie in the transition from the east to ESE striking strike-slip segments to the more north to NE striking thrust segments (these segments are indicated by lines of alternating color in Figure 4b).

6. Seismic Imaging and Interpretations

[17] One of the major aims of the seismic survey was to investigate whether the Hermes Basin formed as a result of pull-apart tectonics, and if so, how? Picking the seafloor reflection of the 3-D seismic data resulted in a 5 m horizontal resolution bathymetry grid. We were able to use this seafloor surface to extract trace-to-trace similarity at (and immediately below) the seafloor. Figure 5, showing both high-resolution bathymetry (Figure 5a) and seismic similarity that was extracted just beneath the seafloor (Figure 5b), was used for a surface-based structural interpretation of the basin. The seafloor trace of the Hermes Fault can be clearly seen to the east of the basin, where it is an extension of the southeastern margin of the basin (Figure 5d).

The improved bathymetric resolution, combined with the similarity extraction, highlights the well-defined northwestern basin margin (striking 076°), which is subparallel to the southeastern margin (striking 083°). The southwestern margin is at the edge of our seismic cube, but it seems to be sub-linear with a mean strike of 102° . It is characterized by numerous arcuate depressions that appear to be the result of surficial slumping. The northeastern margin of the basin (average strike of 110°) includes a significantly larger arcuate depression. The greater basin itself occupies an area of approximately 2.6 km^2 . The steepest basin walls (up to 25°) are directly south and north of the basin center. Linear fabrics that extend into the basin between the two Hermes Fault segments are interpreted as step over strike-slip faults that partially link these two fault segments [e.g., *McClay and Dooley, 1995; Dooley and McClay, 1997; Wu et al., 2009*] (Figure 5d). Lineations that are oblique to and merge with the Hermes Fault segments are likely to be the result of Riedel shear along the strike-slip shear zones [e.g., *Wu et al., 2009*] (Figure 5d).

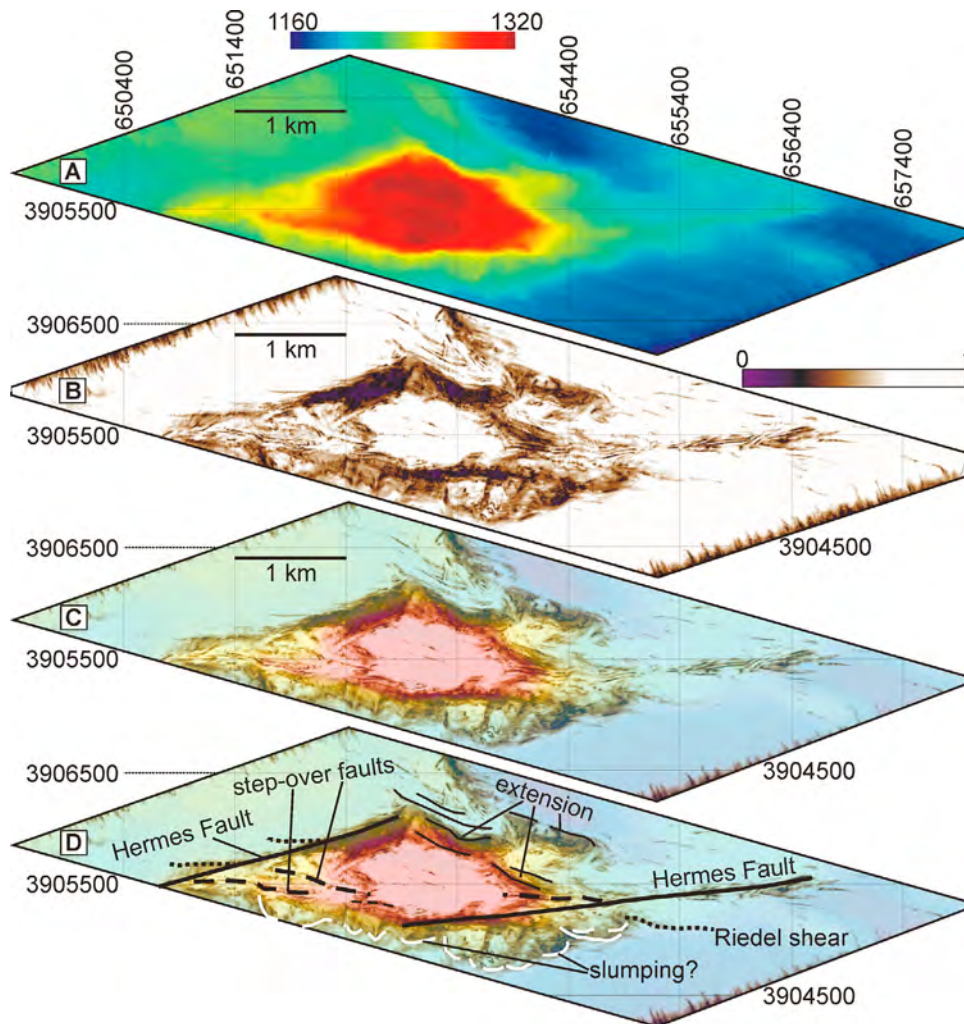


Figure 5. (a) Depth plot (scale in meters below sea level) of the Hermes Basin as determined by picking the seafloor reflection. (b) Seismic similarity attribute calculated directly beneath the seafloor. White regions represent areas where neighboring traces are relatively similar. Brown, through black to purple, highlights areas of progressively lower trace-to-trace similarity. (c) A 50% transparent depth plot (Figure 5a) overlaid on the similarity plot of Figure 5b. (d) Same plot as Figure 5c but with prominent structural lineations annotated: Hermes Fault (heavy black lines), Riedel shears (dotted lines), step over faults (dashed black lines), slump scars (white lines), and extension region (thin black lines).

[18] While the northwestern and southeastern margins are defined by the Hermes strike-slip fault that can be regionally traced in swath bathymetry data (e.g., Figure 3e), the southwestern and northeastern margins are local features. They do not extend away from the basin. It is on these margins where one would expect to find normal faulting that has formed to accommodate the extension driven by dextral motion on the strike-slip faults. The following paragraphs discuss seismic sections extracted from the cube to reveal deformation across all basin margins.

[19] The seismic cube was interpreted in three dimensions with the Kingdom Suite seismic interpretation software. A seismic line oriented NW-SE across the basin shows relatively flat-lying and undeformed strata underlying the seafloor either side of the basin (Figure 6). However, subtle folding of deeper strata is observed on the western side of the basin (Figure 6c). On both sides of the basin, the shallowest layers converge with the basin walls, and at greater depths these strata terminate abruptly rather than continuing underneath the basin. This termination of reflectivity can be seen

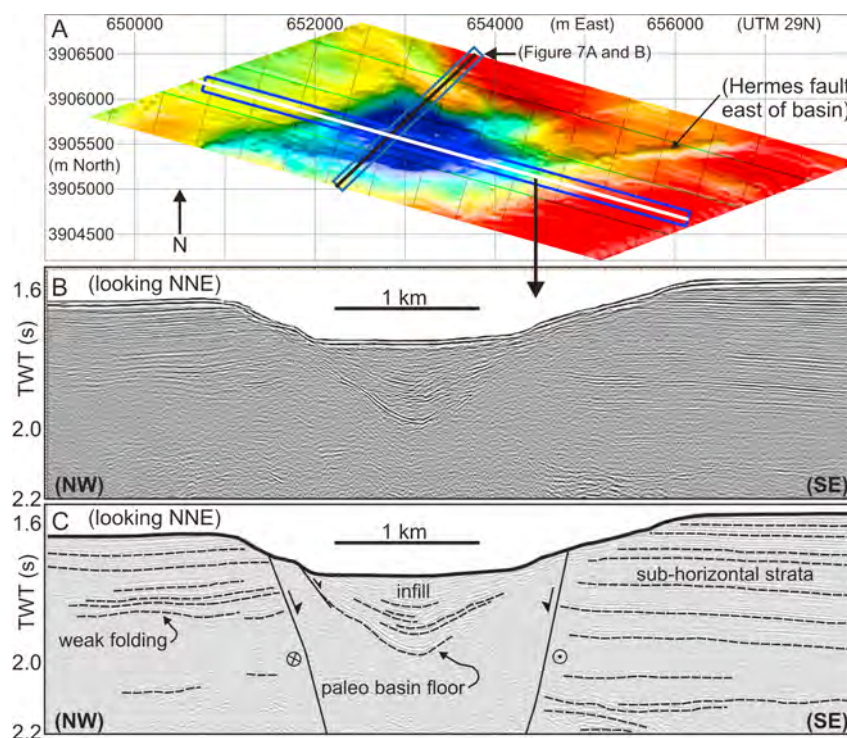


Figure 6. (a) Seafloor surface of the seismic cube plotted in UTM Zone 29N coordinates. The white line (striking ESE) shows the location of the seismic section displayed in Figures 6b and 6c. The black line (striking NE) shows the locations of the seismic section displayed in Figure 7. (b) ESE striking seismic section extracted from the seismic cube. Note that vertical exaggeration at the seafloor is ~ 3.2 . (c) Interpretation overlain on the seismic data.

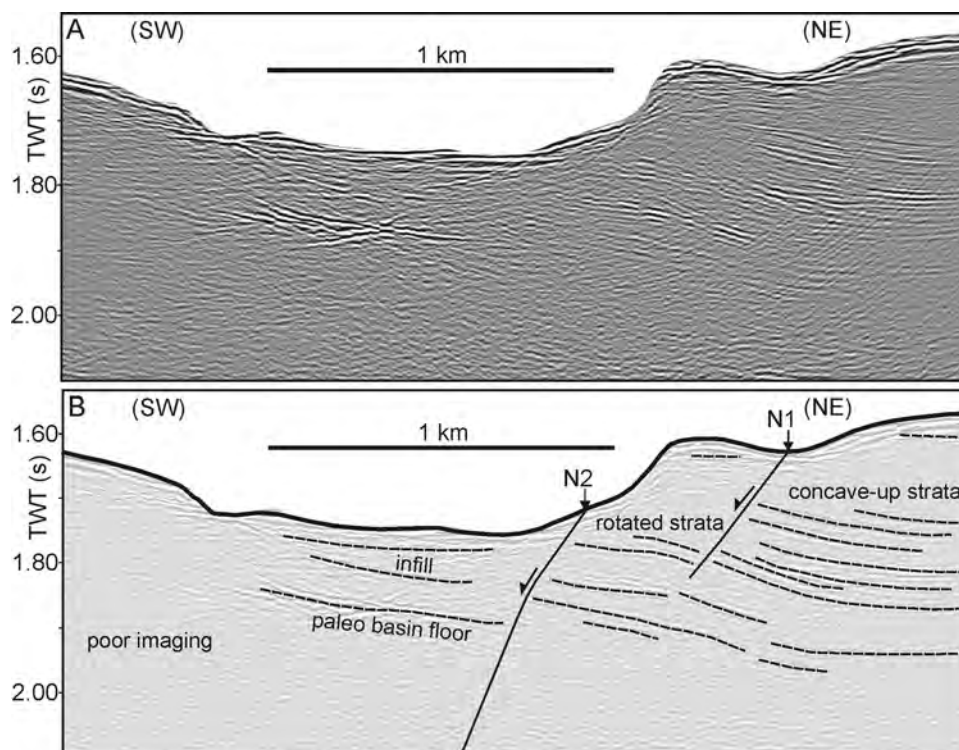


Figure 7. (a) NE striking seismic section extracted from the seismic cube. Note that vertical exaggeration at the seafloor is ~ 3.2 . (b) Interpretation overlain on the seismic data.

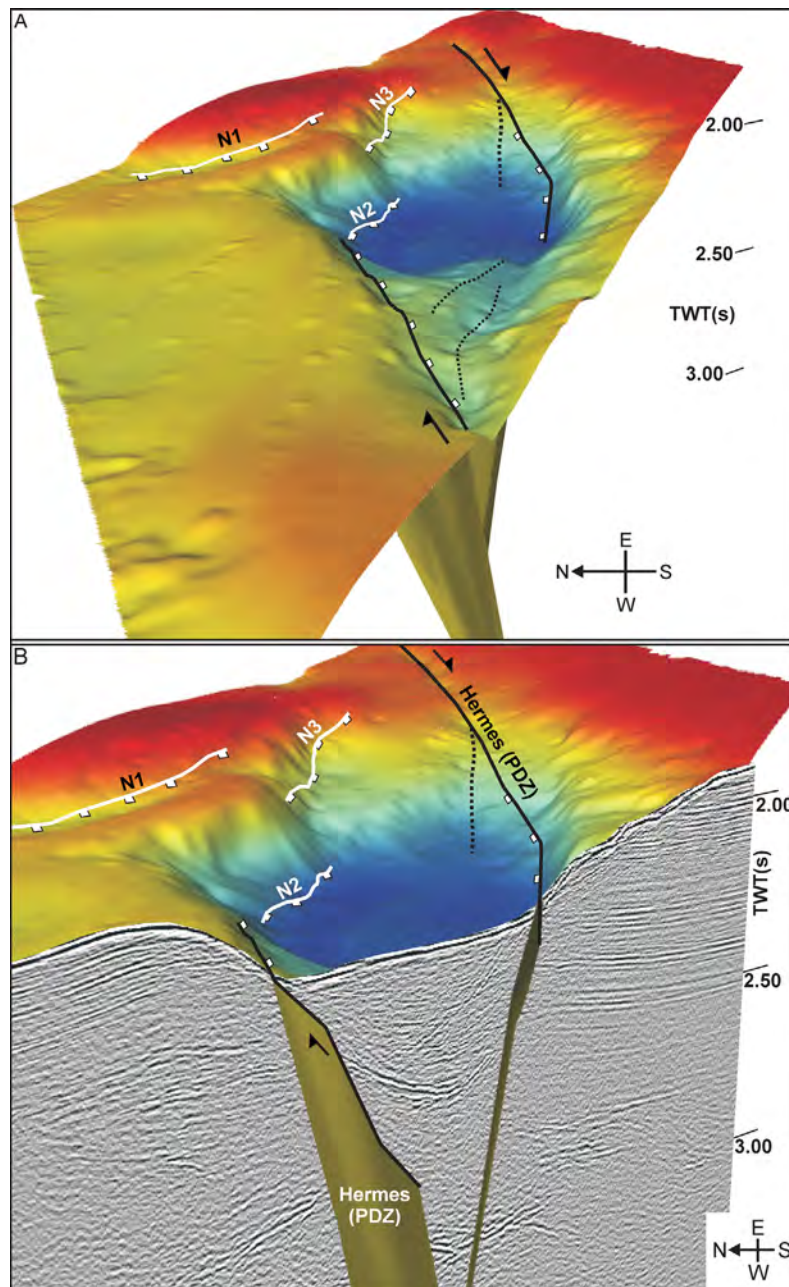


Figure 8. (a) Three-dimensional perspective view of the Hermes Basin. Black lines on the seafloor show the positions of the Hermes fault segments that bound the basin – these are interpreted as the PDZs. White lines show the positions of oblique basin bounding normal faults (N1, N2, and N3). Thin dotted lines show the positions of interpreted step over strike-slip faults (as highlighted in Figure 5) that partially link the two PDZs. (b) The same perspective view as in Figure 8a, but with an arbitrarily cut vertical section showing a gray scale plot of seismic data.

throughout the cube and is interpreted, on both the northwestern and southeastern sides, as the position of the major strike-slip faults that define the northwestern and southeastern basin margins. These fault surfaces, dipping steeply toward the basin, are interpreted to accommodate dextral strike-slip motion – the sense of shear required for pull-apart

basin formation, given the right-stepping fault geometry that was highlighted in Figure 5. Additionally, normal motion overprints the dextral motion to accommodate the extension involved in the opening of the basin.

[20] A very strong positive polarity reflection with an arcuate, concave-up expression is observed



approximately 200 ms beneath the center of the basin floor (Figures 6b and 6c). A package of several other coherent reflections is observed between the major basal arcuate reflection and the seafloor. The basal reflection is interpreted as a paleobasin floor (Figure 6c), and the section above is likely to be in-filled strata that have been sourced from erosion of the steep-sided walls or from sediment transported from elsewhere on the surface of the wedge. The flexural character of the basin fill may reflect differential synsedimentary subsidence of the basin floor [e.g., Hurwitz *et al.*, 2002] – i.e., the center of the basin subsides more rapidly than the margins. Some disruption of the in-filled strata is also visible, which may be associated with deformation during basin evolution.

[21] Figure 7 displays a seismic section oriented NW-SE through the cube. It shows the structural architecture from the southwest margin of the basin, through the basin itself, and across the northeast margin. The northeast margin of the basin is better imaged than the southwest margin, as there is better data coverage on that side. Concave-up strata that are offset and rotated as they approach the basin from the northeast give evidence for normal faulting (fault labeled N1, Figure 7b). Rotated strata indicate block rotation. Further basinward, another fault is interpreted (N2, Figure 7b) between the paleobasin floor (same feature identified in Figure 6c) and the termination of strata observed to the northeast. A third normal fault (N3), farther east of this section, was also identified on the basis of truncated reflectivity beneath a pronounced seafloor slope change. The position of N3 is shown in Figure 8, which is discussed in the following section. Poor imaging and limited data extent in the southwestern reaches of the cube preclude interpretation. It is not possible to say whether normal faulting also occurs on this side of the basin.

[22] Although there are numerous other seafloor depressions elsewhere within the accretionary wedge that have likely formed as a result of dissolution and/or diapiric processes [Gutscher *et al.*, 2009a], the Hermes Basin exhibits several key features that support the interpretation that it is a tectonic pull-apart structure: (1) It lies along a fault line that is offset from one side of the basin to the other. (2) It has a classic rhomboidal shape typical of pull-apart basins (as opposed to subcircular dissolution depressions). (3) Step over faults that partially link basin-bounding fault segments are observed, as they often are in sandbox modeling studies. (4) Continuous reflections at depth either

side of the basin are truncated against the downward projection of the basin boundaries. These truncations are interpreted as the continuations of fault zones beneath the seafloor.

7. Discussion

7.1. Pull-Apart Basin Architecture

[23] Interpretation of the seismic cube reveals the architecture of the Hermes Basin in three dimensions (Figure 8). The Hermes Fault segments dip steeply toward each other, and within the basin region these faults are likely to accommodate some degree of normal motion as well as strike-slip shear. As these faults dip toward each other, it is possible that they merge together at greater depth beneath the basin. The normal faults shown in Figure 8b (labeled N1–N3) accommodate the extension that is imposed on that region of the basin by strike-slip movement on the Hermes faults. Rather than just one major normal fault, these three normal faults (N1, N2 and N3) collectively relieve normal stress on the northeastern margin of the basin.

[24] It is useful to compare the structural features of the Hermes Basin with analog modeling results of pull-apart basin formation [McClay and Dooley, 1995; Dooley and McClay, 1997; Wu *et al.*, 2009]. The strike-slip faults that enter the pull-apart basin from the west and east (i.e., the Hermes Fault) are referred to as the principal displacement zones (PDZs) [McClay and Dooley, 1995] (Figure 8b). The offset of these PDZs and the dextral shear motion along them provide the geometrical configuration and driving force, respectively, for basin development. Within the basin itself, the PDZs continue to undergo strike-slip motion but are also overprinted by extensional motion – indicated in Figure 8b by the normal fault markers within the basin on the Hermes faults. Additionally, normal faults (N1–N3 in Figure 8b) develop oblique to the PDZs to accommodate extensional strain that develops as the basin grows [Wu *et al.*, 2009]. There is evidence for step over strike-slip faulting joining the two offset PDZs in the Hermes Basin (Figure 5d). Such a feature is often formed during analog modeling of pull-apart basin development [e.g., McClay and Dooley, 1995; Rahe *et al.*, 1998; Wu *et al.*, 2009], but is not always observed in natural examples [e.g., Carton *et al.*, 2007].

[25] The Hermes Basin, rhomboidal in shape with steep basin walls that flank a flat basin floor, exhibits a similar expression to the pull-apart basin



in the northern Argentinean Andes presented by *McClay and Dooley* [1995]. The marked reduction in reflectivity coherence at the fault bound margins of the Hermes Basin (Figure 6) is similarly observed in the southern part of the Vienna Basin [*Hinsch et al.*, 2005]. Additionally, concave-up reflections beneath the basin center (Figure 6c) and rotated fault blocks on the basin margin (Figure 7b) are also observed in the southern Vienna Basin. Although concave-up strata are often imaged in pull-apart basins [e.g., *Hurwitz et al.*, 2002; *Hinsch et al.*, 2005; *Carton et al.*, 2007], it should be noted that other pull-apart basins can be characterized by subhorizontal strata or strata that dip downward toward the basin walls [*ten Brink and Ben-Avraham*, 1989]. In such a case, strata were likely tilted by block rotation as the basin pulled apart.

7.2. Fault and Basin Geometry: Implications for Large-Scale Deformation in the Gulf of Cadiz

7.2.1. Strike-Slip Faulting Within the Southern Lobe

[26] A prominent pattern of regional lineaments in the high-resolution bathymetry of the Gulf of Cadiz has been interpreted as the seafloor expression of strike-slip faulting [*Rosas et al.*, 2009; *Zitellini et al.*, 2009]. The existence of basins within the Southern Lobe at locations where such seafloor lineaments step to one side (e.g., the Hermes Basin) strongly supports the interpretation that the lineaments are indeed strike-slip faults and the basins have formed by pull-apart tectonics.

[27] The 3-D seismic data suggest that the Hermes Basin formed as a result of dextral shear. Several other basins located on fault offsets (Figure 2) provide an additional opportunity to check the sense of shear required on each of these other faults for basin formation. To test this, we modeled a simplified strain distribution that would result from an arbitrary amount of slip on the network of strike-slip faults using the Coulomb 3.1 program [*Lin and Stein*, 2004; *Toda et al.*, 2005]. Our modeling scenario is purely qualitative because we are only interested in the distribution of extension and compression (Figure 9). Our first model assumed dextral motion (Figure 9c), as this is the interpreted sense of shear on the SWIM faults [*Rosas et al.*, 2009; *Zitellini et al.*, 2009] and also the predicted sense on the Hermes Fault. Pull-apart basins should only occur where the strain distribution is dilatational (i.e., blue). Although this

dextral strike-slip model satisfies the pull-apart basins in the northern part of the lobe (basins c and d), the basins to the south (basins e, f and g) occur where the strain distribution is compressional (Figure 9c). This problem is resolved by changing the sense of shear on the southern faults (i.e., those faults to the right of the dotted line in Figure 9d) to sinistral. Therefore, we interpret the northern faults in the Southern Lobe as dextral and the southern faults as sinistral. Figure 10 shows enlarged views of the seafloor bathymetry around these three southern basins (e, f, and g) where we predict sinistral motion.

7.2.2. Processes Driving Strike-Slip Faulting in the Southern Lobe

[28] It has been argued that strike-slip faulting in the Gulf of Cadiz is occurring in response to the modern inception of a dextral strike-slip plate boundary due to the oblique collision of Nubia and Iberia [*Rosas et al.*, 2009; *Zitellini et al.*, 2009]. *Rosas et al.* [2009] provided good evidence, in the form of surface deformation in analog models that mimicked natural seafloor topography, for dextral motion along strike-slip faults immediately to the northwest of the accretionary wedge (Figure 1). *Zitellini et al.* [2009] expanded these results and interpreted, together with the fault segments outlined by *Rosas et al.* [2009], a larger set of lineations exhibiting similar strike directions (WNW-ESE) as dextral strike-slip faults – the SWIM faults (Figure 1). However, closer inspection in this study of seafloor fault expressions within the Southern Lobe of the upper accretionary wedge indicates that some of the faults (including the Southern SWIM Fault) accommodate sinistral motion. Our interpretations contradict those of *Zitellini et al.* [2009], who suggest that dextral motion is ubiquitous and extends into the Southern Lobe. This opposing sense of shear observed on a local scale suggests that these faults within the Southern Lobe are not deforming in response to movement along a dextral transform plate boundary. If this were the case, then all faults that are subparallel to the proposed transform plate boundary (i.e., those faults highlighted red in Figure 2b) should exhibit a dextral sense of shear. Of course, with conjugate faulting, faults of opposite shear sense exist in close proximity, but such fault patterns orientate themselves at angles of approximately 60° to each other [*Sylvester*, 1988]. The Northern and Southern SWIM Faults in the Southern Lobe are subparallel to each other and have opposite shear sense; they are not conjugate faults. The stark difference in

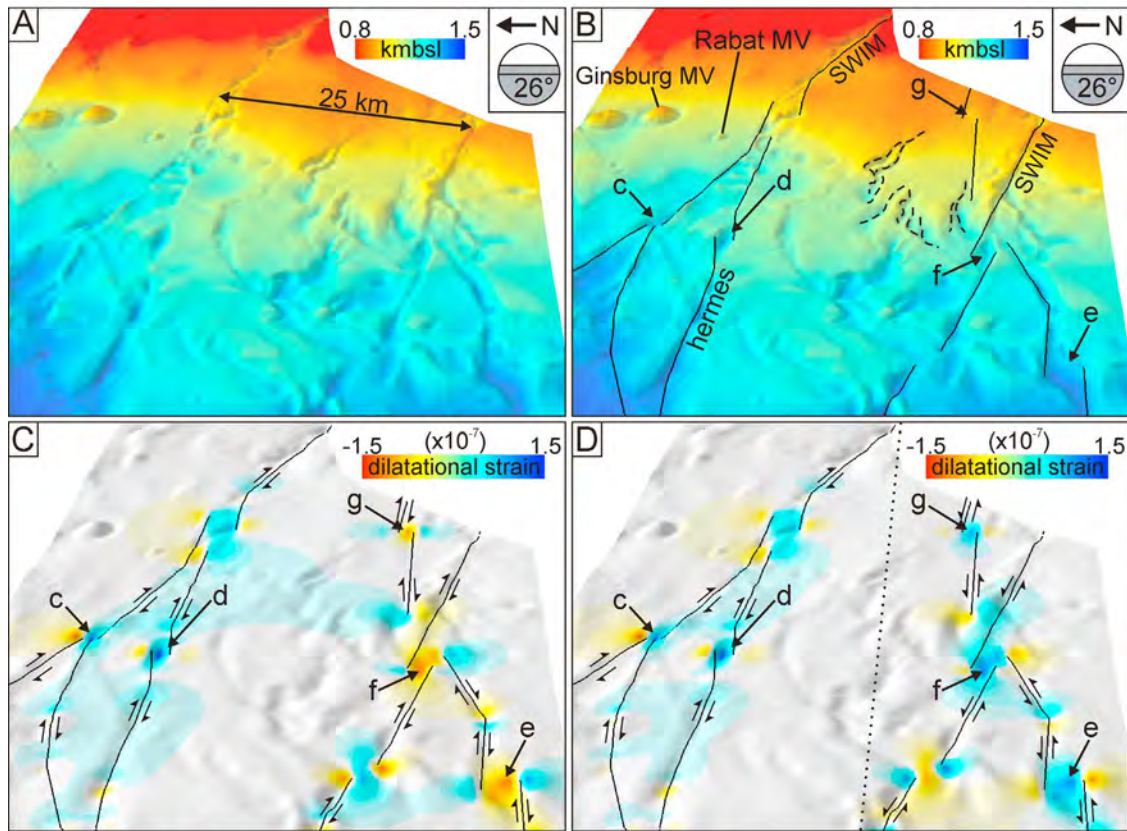


Figure 9. Summary of strain modeling around strike-slip faults in the Southern Lobe. Coulomb 3.1's default parameterization for Poisson's ratio (0.25), Young's modulus (8×10^5 bars), and the friction coefficient (0.4) was adopted. Idealized linear fault segments were digitized, assumed to be vertical, and assigned an arbitrary amount of pure strike-slip motion (0.5 m). (a) Three-dimensional perspective view of shaded bathymetry illuminated from the north. The north arrow and the inclinometer describe the orientation of the view. (b) Same as Figure 9a but with interpretations. Dashed black lines are channel systems. Black lines are the idealized linear fault segments that approximate the interpreted trends of strike-slip faults (SWIM faults and the Hermes fault are labeled). Arrows labeled c, d, e, f, and g point to interpreted pull-apart basins (see Figure 2b). (c) Dilatational strain calculated for the area by assuming an equal arbitrary amount of slip (0.5 m) on each strike-slip fault segment (shear sense indicated by arrows; note that all are dextral). Basins e, f, and g show compression in this model. (d) Dilatational strain calculated for the area by assuming 0.5 m of strike slip on each fault segment. In contrast to Figure 9c, the group of faults to the south (all those to the right of the dotted line) undergo sinistral shear. All basins are now in zones of dilatation.

appearance between the Southern Lobe faults and dextral transform faults further west [e.g., Rosas *et al.*, 2009], highlighted in the comparison between Figures 1b and 1c, also adds credence to the interpretation that the Southern Lobe faults have been formed by a different driving mechanism – presumably more recently, on account of the younger appearance. Barnes *et al.* [2001] noted that pull-apart basins on an offshore segment of the Alpine Fault in New Zealand may be ephemeral in the geological record, being progressively developed and destroyed over time scales of 10^5 – 10^6 years [Zhang *et al.*, 1989; Sibson, 1986]. Should the fault-basin pattern in the Southern Lobe also only exist over relatively short time scales, this

would give further support to the interpretation that the faulting is very recent in origin.

[29] To evaluate plausible mechanisms for development of the opposite strike-slip shear sense, it is essential to consider how stress fields can be sufficiently heterogeneous on a relatively small scale. By measuring in situ stress states from borehole wall failures in the Nankai accretionary wedge, Chang *et al.* [2010] found the maximum horizontal stress component (S_{Hmax}) of two boreholes located approximately 10 km apart were almost perpendicular to each other. They suggested that the compressive tectonic force due to the convergence of the Philippine Sea Plate against the Eurasian

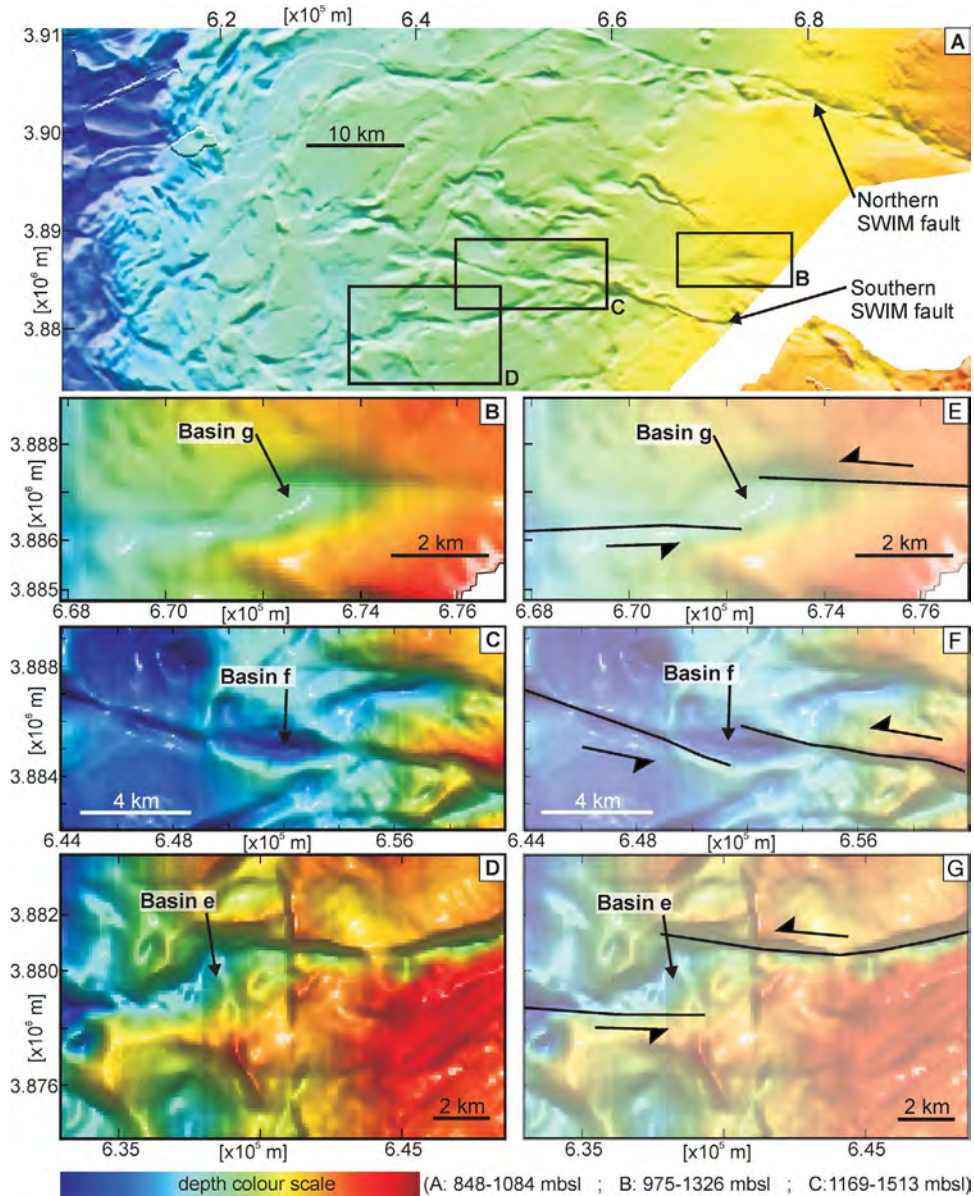


Figure 10. (a) High-resolution bathymetry in the Southern Lobe. The Northern and Southern SWIM Faults are labeled, as are three boxes that show the extents of enlarged fields of view given around basins in Figures 1b–1d. (b–d) Enlarged bathymetry plots around “Basin g,” “Basin f”, and “Basin e”, respectively (basin nomenclature follows that of Figure 2b). (e–g) Interpretations of Basin g, Basin f, and Basin e, respectively. The basins are interpreted to have formed by movement along left-stepping sinistral strike-slip faults.

Plate is not uniformly propagated into the wedge. Instead, they inferred that local deformation caused by factors such as (1) gravitational extension in the fore arc [e.g., King *et al.*, 2010; Willett, 1999] and (2) thrusting and bending within individual geologic domains in the wedge [e.g., Cai *et al.*, 1995] has influenced pronounced changes in the stress field.

[30] The following observations and interpretations of tectonic style in the Southern Lobe provide

insight into the case of the Gulf of Cadiz accretionary wedge:

[31] 1. Normal faults have been imaged in 2-D seismic data in the upper part of the wedge [Gutscher *et al.*, 2009a] and further upslope on the Moroccan Margin [Flinch, 1994]. The focusing of mud volcano fields on the upper slope of the wedge may also be correlated with extensional faulting in this region [Medialdea *et al.*, 2009].



[32] 2. Morphological evidence of raft tectonics and gravitational instabilities on the upper wedge led *Gutscher et al.* [2009a] to interpret that the upper wedge is undergoing gravitational spreading on top of a weak, very shallow-dipping upper detachment – possibly explained by a salt layer [*Gutscher et al.*, 2009a; *Heeschen et al.*, 2008].

[33] 3. The deformation front of the Southern Lobe exhibits some of the steepest slopes of the entire surface expression of the accretionary wedge, and there is evidence for a link between thrusting at the deformation front and strike-slip faulting further upslope (Figure 4).

[34] We suggest that the opposing shear senses on strike-slip faults could be driven by a spatial variance in the rates of accretion at the deformation front, or in the rates of extension and gravitational sliding occurring farther upslope. Both scenarios require spatial differences in the degree of coupling: in the case of accretion, on the thrust interfaces, or in the case of gravitational sliding, on the low-angle detachment surface. Such variations can be envisaged in various ways, including (1) variations in pore fluid pressure (altering the effective stress on slip planes [*Hubbert and Rubey*, 1959]), (2) the distribution of salt as a weak layer [e.g., *Marshak*, 2004], or (3) the distribution of asperities/localized structures that can increase the coupling on slip planes [e.g., *Wang*, 1995]. In relation to the latter point, existing studies have underscored the influence of localized structures on the downgoing plate on varying deformation styles within the wedge [e.g., *Dominguez et al.*, 2000; *Graindorge et al.*, 2008; *Marshak*, 2004]. It may be feasible that distinct structures being subducted beneath the Gulf of Cadiz accretionary wedge are causing pronounced spatially variant deformation rates in the overlying sediments.

[35] A global compilation of natural fold and thrust belts and sandbox modeling of surface deformation fabrics [*Macedo and Marshak*, 1999; *Marshak*, 2004] has given insight into the importance of the geological setting on the geometrical arrangement of surface structural trend lines (i.e., the trends of folds and faults in plan view). Relationships between the leading edge of the fold and thrust belt and the internal trend lines differ for systems that have formed from (1) the interaction of asperities at colliding margins and (2) those that have formed above a basal detachment whose strength varies laterally along strike. Colliding asperities result in trend lines that diverge away from the limbs of the leading edge, whereas trend lines in deforming

sediments above detachments converge toward the limbs of the leading edge [*Macedo and Marshak*, 1999]. Figure 11a shows a structural sketch the Sulaiman fold and thrust belt in Pakistan, whose form was governed by the presence of a sedimentary glide horizon [*Marshak*, 2004]. Trend lines converge toward the limbs of the leading edge, and subparallel strike-slip faults within the deformed region exhibit opposite shear senses. Although the scale in the Southern Lobe of this study is significantly smaller, several similar features should be noted (comparing Figures 11a and 11b). The leading edge in the case of the Southern Lobe is its deformation front. Fold/thrust ridges within the lobe exhibit a convergence toward the leading edge (deformation front), and strike-slip faults of opposite shear sense cut through the lobe (Figure 11b). These similarities indicate that differential sliding rates upon a weak basal detachment is certainly a feasible driving force for the interpreted strike-slip faulting patterns in the Southern Lobe.

[36] The simplified sketch in Figure 11c conceptually shows our model of deformation processes in the Southern Lobe. Strike-slip faults accommodate spatial differences in rates of accretion and/or upslope rates of extension and sliding upon a weak basal detachment. Adjacent blocks move at different rates, inducing a shearing that is accommodated by strike-slip faults. The model incorporates existing interpretations of deformation in the upper part of the Gulf of Cadiz's accretionary wedge, and satisfies the new interpretations of shear sense on strike-slip faults in the Southern Lobe. For the sake of simplicity, we only show two strike-slip faults and one thrust sheet in Figure 11c. In reality, we predict that an array of strike-slip and thrust deformation collectively relieves the spatially variant strain.

[37] This study highlights the importance of close analysis of modern seafloor structures and deformation patterns for the understanding of regional processes in the Gulf of Cadiz. We have shown evidence that the dextral strike-slip faults on the upper slope of the Southern Lobe are part of a tectonic system of both dextral and sinistral strike-slip faults that are linked by a ridge system at the toe of the lobe. Recent movement on these faults does not appear to be related to the proposed development of a modern dextral transform plate boundary aligned along the SWIM faults [*Zitellini et al.*, 2009], but to laterally changing senses of motion most easily explained by spatially variant gravitational tectonics or accretion rates. This removes an important piece of evidence for an

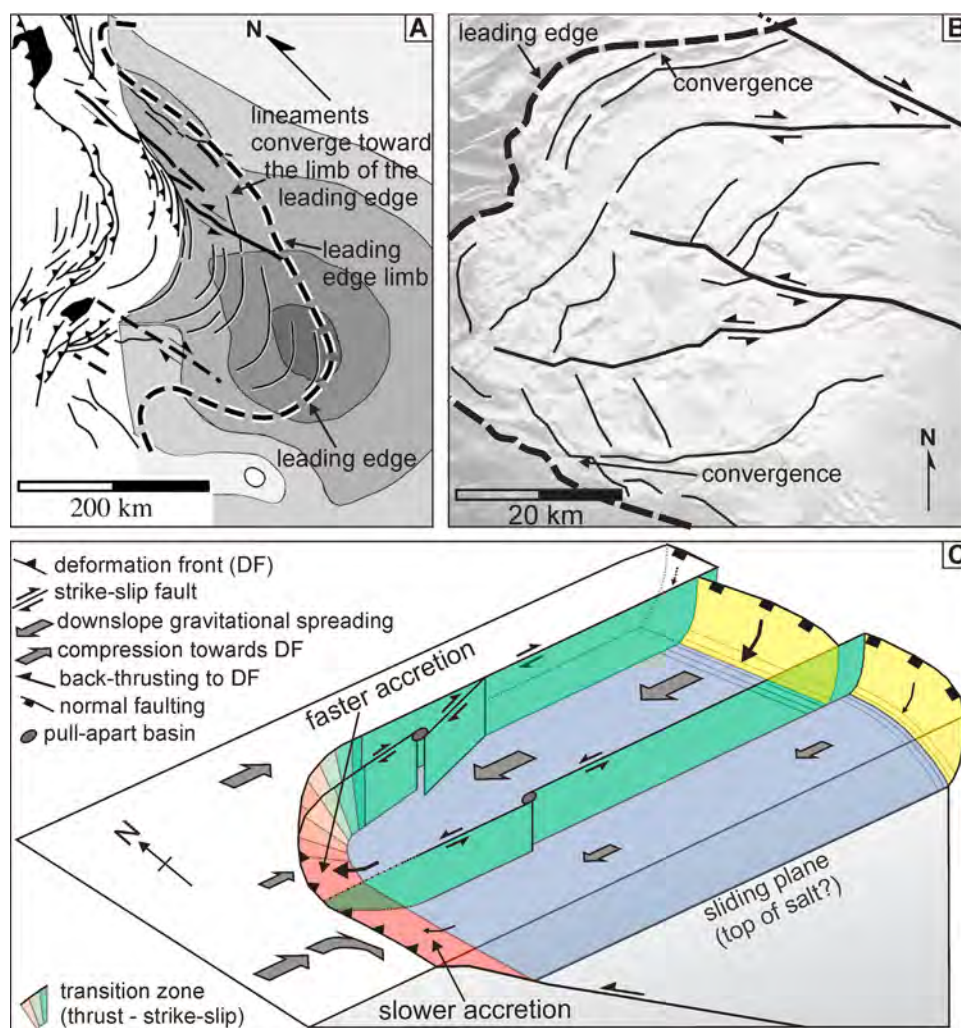


Figure 11. (a) Structural lineaments in the Sulaiman salient, Pakistan, where movement above a basal glide horizon of varying spatial strength has caused such a surface structural pattern [after *Marshak*, 2004]. (b) Structural lineaments in the Southern Lobe, where we also suggest that basal sliding may vary spatially. (c) Conceptual diagram showing the interpreted link that strike-slip faulting within the Southern Lobe provides between accretion (to the west) and extension further upslope (to the east). The simplified representation shows varying deformation velocities (indicated by different sized arrows) for adjacent blocks, which induce a shearing between blocks that is accommodated by strike-slip faulting. The strike-slip faults are therefore interpreted to be accommodation structures that relieve strain that accumulates from spatially variant deformation rates.

active dextral transform plate boundary this far south in the Gulf of Cadiz. It is, however, possible (and perhaps even likely, given the common strike direction) that modern faulting in the Southern Lobe has reactivated some older structures related to a transform boundary. Thus, understanding the plate boundary will require further research to distinguish between the transform plate boundary model [*Zitellini et al.*, 2009] and the alternative interpretation of ongoing subduction [*Gutscher et al.*, 2002]. Only this will allow for discovery of the source of the great Lisbon earthquake of

1755. As we suggest that the modern deformation fabrics are related to active deformation within the accretionary wedge, this work supports the model of active subduction west of Gibraltar [*Gutscher et al.*, 2002]. However, it is important to note that our model of a variably collapsing wedge above a weak basal detachment could even take place in the absence of active subduction [e.g., *Bilotti and Shaw*, 2005].

[38] In order to evaluate which of the two scenarios proposed in this paper (i.e., spatially variant accretion rates or spatially variant gravitational



sliding rates) is more likely to be responsible for the observed deformation patterns, deep penetration seismic data would have to be acquired in the area to resolve the deeper structures beneath the Southern Lobe. Future work would benefit from more regional seismic profiles that may help to constrain (1) whether thrust and strike-slip faults share a common detachment surface and (2) slip magnitudes on faults that may show a relationship between the two forms of faulting [Benesh, 2010]. With respect to point 2, Benesh [2010] showed that abrupt changes in strike-slip magnitude in the vicinity of intersections with thrust faults may be used to distinguish between relatively “thin-skinned” strike-slip faults and more conventional deep-seated ones.

8. Conclusions

[39] Active deformation within the Southern Lobe of the upper accretionary wedge in the Gulf of Cadiz has been examined from high-resolution swath bathymetry data and 3-D seismic data centered over a pull-apart basin. The eastern part of the lobe is multiply dissected by relatively linear fault segments, including two dominant ESE trending SWIM faults (nomenclature after Zitellini *et al.* [2009]). Several basins observed at bends in these faults, which are interpreted locations of pull-apart tectonics, support previous interpretations that these fault segments are strike-slip in nature.

[40] Detailed analysis of the Hermes Basin indicates that it formed as a result of a right-stepping bend in a dextral strike-slip fault. The basin architecture shows many similarities to other natural pull-apart basins [e.g., McClay and Dooley, 1995] and also to sand box modeling results [e.g., Wu *et al.*, 2009].

[41] There is strong evidence from bathymetric lineaments for a link between compressional structures at the deformation front of the Southern Lobe and strike-slip faulting further to the east (Figure 4). These lineaments indicate that accretion and strike-slip processes are occurring simultaneously.

[42] While the Northern SWIM fault in the Southern Lobe is interpreted as dextral, faults farther south appear to accommodate sinistral strike-slip motion. The surface features in the lobe likely reveal complex deformation that is influenced by upslope extension [Flinch, 1994; Gutscher *et al.*, 2009a] and downslope compression – two processes linked by strike-slip faulting that appears to accommodate spatial variance in deformation rates.

[43] Comparison of 2-D migrated and 3-D migrated data from the pull-apart basin area shows that 3-D seismic data are required to image targets of small scale lateral heterogeneity. In this study, the 3-D data were collected using the P-Cable system during a period of three days showing that it is both feasible and efficient to conduct such surveys with normal research vessels.

Acknowledgments

[44] We thank Michael Stipp (IFM-GEOMAR) for discussions on the structural geology of pull-apart basins. We gratefully acknowledge the constructive reviews of Uri ten Brink, Richard Norris, Chris Guzowski, and two earlier anonymous reviewers, which significantly helped us to improve the manuscript. We also thank editor Thorsten Becker for the handling of the manuscript. This work was funded by the EC through the HERMES project (GOCE-CT-2005-511234-1). We thank the master and the crew of RRS Charles Darwin and Frode Eriksen (VBPR) for crucial support during the voyage CD178. Seismic processing utilized a variety of programs, including Seismic Unix, Matlab, RadexPro and Western Geco’s OMEGA2. Three-dimensional seismic interpretation and visualization were carried out with OpenDtect and The Kingdom Suite. Bathymetry surface analysis techniques were carried out with ArcGIS and GMT.

References

- Barnes, P. M., R. Sutherland, B. Davy, and J. Delteil (2001), Rapid creation and destruction of sedimentary basins on mature strike-slip faults: An example from the offshore Alpine Fault, New Zealand, *J. Struct. Geol.*, 23(11), 1727–1739, doi:10.1016/S0191-8141(01)00044-X.
- Benesh, N. P. (2010), The mechanics of fault-bend folding and tear-fault systems in the Niger Delta, 124 pp, Ph.D. thesis, Harvard Univ., Cambridge, Mass.
- Bilotti, F., and J. H. Shaw (2005), Deep-water Niger Delta fold and thrust belt modeled as a critical-taper wedge: The influence of elevated basal fluid pressure on structural styles, *AAPG Bull.*, 89(11), 1475–1491, doi:10.1306/06130505002.
- Cai, Y., C.-Y. Wang, W.-T. Hwang, and G. R. Cochrane (1995), The effect of fault-bend folding on seismic velocity in the marginal ridge of accretionary prisms, *Pure Appl. Geophys.*, 145(3–4), 637–646, doi:10.1007/BF00879593.
- Calvert, A., E. Sandvol, D. Seber, M. Barazangi, S. Roecker, T. Mourabit, F. Vidal, G. Alguacil, and N. Jabour (2000), Geodynamic evolution of the lithosphere and upper mantle beneath the Alboran region of the western Mediterranean: Constraints from travel time tomography, *J. Geophys. Res.*, 105, 10,871–10,898, doi:10.1029/2000JB900024.
- Carton, H., et al. (2007), Seismic imaging of the three-dimensional architecture of the Çınarcık Basin along the North Anatolian Fault, *J. Geophys. Res.*, 112, B06101, doi:10.1029/2006JB004548.
- Chang, C., L. C. McNeill, J. C. Moore, W. Lin, M. Conin, and Y. Yamada (2010), In situ stress state in the Nankai accretionary wedge estimated from borehole wall failures, *Geo-*



- chem. Geophys. Geosyst.*, *11*, Q0AD04, doi:10.1029/2010GC003261.
- Dewey, J. F., M. L. Helman, E. Turco, D. H. W. Hutton, and S. D. Knott (1989), Kinematics of the western Mediterranean, in *Alpine Tectonics*, edited by M. P. Coward, D. Dietrich, and R. G. Park, *Geol. Soc. Spec. Publ.*, *45*, 265–283.
- Dominguez, S., J. Malavieille, and S. E. Lallemand (2000), Deformation of accretionary wedges in response to seamount subduction: Insights from sandbox experiments, *Tectonics*, *19*(1), 182–196, doi:10.1029/1999TC900055.
- Dooley, T., and K. McClay (1997), Analogue modelling of pull-apart basins, *AAPG Bull.*, *81*, 1804–1826.
- Flinch, J. F. (1994), Tectonic evolution of the Gibraltar Arc, 813 pp, Ph.D. thesis, Rice Univ., Houston, Tex.
- Grácia, E., J. J. Dañoibeitia, and J. Vergés, and the PARSIAL Team (2003), Mapping active faults offshore Portugal (36°N–38°N): Implications for seismic hazard assessment along the southwest Iberian margin, *Geology*, *31*, 83–86, doi:10.1130/0091-7613(2003)031<0083:MAFOPN>2.0.CO;2.
- Graindorge, D., et al. (2008), Impact of lower plate structure on upper plate deformation at the NW Sumatran convergent margin from seafloor morphology, *Earth Planet. Sci. Lett.*, *275*, 201–210, doi:10.1016/j.epsl.2008.04.053.
- Gutscher, M. A. (2004), What caused the Great Lisbon earthquake?, *Science*, *305*, 1247–1248, doi:10.1126/science.1101351.
- Gutscher, M. A., J. Malod, J. P. Rehault, I. Contrucci, F. Klingelhoefer, L. Mendes-Victor, and W. Spakman (2002), Evidence for active subduction beneath Gibraltar, *Geology*, *30*(12), 1071–1074, doi:10.1130/0091-7613(2002)030<1071:EFASBG>2.0.CO;2.
- Gutscher, M.-A., et al. (2009a), Tectonic shortening and gravitational spreading in the Gulf of Cadiz accretionary wedge: Observations from multi-beam bathymetry and seismic profiling, *Mar. Pet. Geol.*, *26*(5), 647–659, doi:10.1016/j.marpetgeo.2007.11.008.
- Gutscher, M.-A., S. Dominguez, G. K. Westbrook, and P. Leroy (2009b), Deep structure, recent deformation and analog modeling of the Gulf of Cadiz accretionary wedge: Implications for the 1755 Lisbon earthquake, *Tectonophysics*, *475*, 85–97, doi:10.1016/j.tecto.2008.11.031.
- Heeschen, K., M. Haeckel, C. Berndt, D. Teagle, M. Palmer, D. Green, M. Cooper, H. Vanneste, and V. Liebetrau (2008), Origin of fluids and salts at the Mercator mud volcano, Gulf of Cadiz, paper presented at EGU General Assembly, Vienna, 13–18 April.
- Hinsch, R., K. Decker, and H. Peresson (2005), 3-D seismic interpretation and structural modeling in the Vienna Basin: Implications for Miocene to recent kinematics, *Austrian J. Earth Sci.*, *97*, 38–50.
- Hubbert, M. K., and W. W. Rubey (1959), Role of fluid pressure in the mechanics of overthrust faulting, *Geol. Soc. Am. Bull.*, *70*, 115–205, doi:10.1130/0016-7606(1959)70[115:ROFPIM]2.0.CO;2.
- Hurwitz, S., Z. Garfunkel, Y. Ben-Gai, M. Reznikov, Y. Rotstein, and H. Gvirtzman (2002), The tectonic framework of a complex pull-apart basin: seismic reflection observations in the Sea of Galilee, Dead Sea transform, *Tectonophysics*, *359*, 289–306, doi:10.1016/S0040-1951(02)00516-4.
- King, R. C., R. R. Hillis, M. R. P. Tingay, and A.-R. Damit (2010), Present-day stresses in Brunei, NW Borneo: Superposition of deltaic and active margin tectonics, *Basin Res.*, *22*, 236–247, doi:10.1111/j.1365-2117.2009.00407.x.
- Lin, J., and R. S. Stein (2004), Stress triggering in thrust and subduction earthquakes, and stress interaction between the southern San Andreas and nearby thrust and strike-slip faults, *J. Geophys. Res.*, *109*, B02303, doi:10.1029/2003JB002607.
- Loneragan, L., and N. White (1997), Origin of the Betic-Rif mountain belt, *Tectonics*, *16*(3), 504–522, doi:10.1029/96TC03937.
- Macedo, J., and S. Marshak (1999), Controls on the geometry of fold-thrust belt salients, *Geol. Soc. Am. Bull.*, *111*, 1808–1822, doi:10.1130/0016-7606(1999)111<1808:COTGOF>2.3.CO;2.
- Marshak, S. (2004), Salients, recesses, arcs, oroclines, and syntaxes—A review of ideas concerning the formation of map-view curves in fold-thrust belts, in *Thrust Tectonics and Hydrocarbon Systems*, edited by K. R. McClay, *AAPG Mem.*, *82*, 131–156.
- McClay, K., and T. Dooley (1995), Analogue models of pull-apart basins, *Geology*, *23*(8), 711–714, doi:10.1130/0091-7613(1995)023<0711:AMOPAB>2.3.CO;2.
- Medialdea, T., L. Somoza, L. M. Pinheiro, M. C. Fernández-Puga, J. T. Vázquez, R. León, M. K. Ivanov, V. Magalhaes, V. Diaz-del-Río, and R. Vegas (2009), Tectonics and mud volcano development in the Gulf of Cádiz, *Mar. Geol.*, *261*, 48–63, doi:10.1016/j.margeo.2008.10.007.
- Micallef, A., C. Berndt, D. G. Masson, and D. A. V. Stow (2007), A technique for the morphological characterization of submarine landscapes as exemplified by debris flows of the Storegga Slide, *J. Geophys. Res.*, *112*, F02001, doi:10.1029/2006JF000505.
- Platt, J. P., and R. L. M. Vissers (1989), Extensional collapse of thickened continental lithosphere: A working hypothesis for the Alboran Sea and Gibraltar arc, *Geology*, *17*, 540–543, doi:10.1130/0091-7613(1989)017<0540:ECOTCL>2.3.CO;2.
- Rahe, B., D. A. Ferrill, and A. R. Morris (1998), Physical analog modeling of pull-apart basin evolution, *Tectonophysics*, *285*, 21–40, doi:10.1016/S0040-1951(97)00193-5.
- Rosas, F. M., J. C. Duarte, P. Terrinha, V. Valadares, and L. Matias (2009), Morphotectonic characterization of major bathymetric lineaments in Gulf of Cadiz (Africa-Iberia plate boundary): Insights from analogue modelling experiments, *Mar. Geol.*, *261*, 33–47, doi:10.1016/j.margeo.2008.08.002.
- Rosenbaum, G., G. S. Lister, and C. Duboz (2002), Relative motions of Africa, Iberia and Europe during Alpine orogeny, *Tectonophysics*, *359*, 117–129, doi:10.1016/S0040-1951(02)00442-0.
- Sartori, R., L. Torelli, N. Zitellini, D. Peis, and E. Lodolo (1994), Eastern segment of the Azores-Gibraltar line (central-eastern Atlantic): An oceanic plate boundary with diffuse compressional deformation, *Geology*, *22*, 555–558, doi:10.1130/0091-7613(1994)022<0555:ESOTAG>2.3.CO;2.
- Sibson, R. H. (1986), Rupture interaction with fault jogs, in *Earthquake Source Mechanics*, *Geophys. Monogr. Ser.*, vol. 37, edited by D. Shamita, J. Boatwright, and C. H. Scholz, pp. 157–167, AGU, Washington, D. C.
- Sylvester, A. G. (1988), Strike-slip faults, *Geol. Soc. Am. Bull.*, *100*, 1666–1703, doi:10.1130/0016-7606(1988)100<1666:SSF>2.3.CO;2.
- Terrinha, P., et al. (2003), Tsunamigenic-seismogenic structures, neotectonics, sedimentary processes and slope instability on the Southwest Portuguese Margin, *Mar. Geol.*, *195*, 55–73, doi:10.1016/S0025-3227(02)00682-5.



- ten Brink, U. S., and Z. Ben-Avraham (1989), The anatomy of a pull-apart basin: Seismic reflection observations of the Dead Sea Basin, *Tectonics*, *8*(2), 333–350, doi:10.1029/TC008i002p00333.
- Toda, S., R. S. Stein, K. Richards-Dinger, and S. Bozkurt (2005), Forecasting the evolution of seismicity in southern California: Animations built on earthquake stress transfer, *J. Geophys. Res.*, *110*, B05S16, doi:10.1029/2004JB003415.
- Tortella, D., M. Torne, and A. Perez-Estaun (1997), Geodynamic evolution of the eastern segment of the Azores-Gibraltar Zone: The Goringe Bank and Gulf of Cadiz region, *Mar. Geophys. Res.*, *19*, 211–230, doi:10.1023/A:1004258510797.
- Wang, K. (1995), Coupling of tectonic loading and earthquake fault slips at subduction zones, *Pure Appl. Geophys.*, *145*(3–4), 537–559, doi:10.1007/BF00879588.
- Wessel, P., and W. H. S. Smith (1998), New, improved version of the Generic Mapping Tools released, *Eos Trans. AGU*, *79*, 579, doi:10.1029/98EO00426.
- Willett, S. D. (1999), Rheological dependence of extension in wedge models of convergent orogens, *Tectonophysics*, *305*, 419–435, doi:10.1016/S0040-1951(99)00034-7.
- Wilson, M. F. J., B. O’Connell, C. Brown, J. C. Guinan, and A. J. Grehan (2007), Multiscale terrain analysis of multibeam bathymetry data for habitat mapping on the continental slope, *Mar. Geod.*, *30*, 3–35, doi:10.1080/01490410701295962.
- Wu, J. E., K. McClay, P. Whitehouse, and T. Dooley (2009), 4D analogue modelling of transtensional pull-apart basins, *Mar. Pet. Geol.*, *26*, 1608–1623, doi:10.1016/j.marpetgeo.2008.06.007.
- Zhang, P., B. C. Burchfiel, S. Chen, and Q. Deng (1989), Extinction of pull-apart basins, *Geology*, *17*, 814–817, doi:10.1130/0091-7613(1989)017<0814:EOPAB>2.3.CO;2.
- Zitellini, N. (2001), Source of 1755 Lisbon earthquake and tsunami investigated, *Eos Trans. AGU*, *82*, 285–291.
- Zitellini, N., et al. (2009), The quest for the Africa-Eurasia plate boundary west of the Strait of Gibraltar, *Earth Planet. Sci. Lett.*, *280*, 13–50, doi:10.1016/j.epsl.2008.12.005.